Evaluation of Different Numerical Approaches to Modeling Flood Flows Over Groynes

Yildiz, Burhan; Ambagts, Lindert; Yossef, Mohamed F. M.; Mosselman, Erik

DOI
10.1029/2023WR036895

Publication date
2024

Document Version
Final published version

Published in
Water Resources Research

Citation (APA)
Yildiz, B., Ambagts, L., Yossef, M. F. M., & Mosselman, E. (2024). Evaluation of Different Numerical Approaches to Modeling Flood Flows Over Groynes. *Water Resources Research*, *60*(6), Article e2023WR036895. https://doi.org/10.1029/2023WR036895

Water Resources Research

RESEARCH ARTICLE
10.1029/2023WR036895

Evaluation of Different Numerical Approaches to Modeling Flood Flows Over Groynes

Burhan Yildiz[1,2,3], **Lindert Ambagts**[4,5], **Mohamed F. M. Yossef**[3], **and Erik Mosselman**[3,6]

[1]Now at Department of Civil Engineering, Mugla Sitki Kocman University, Mugla, Turkey, [2]Now at Department of Hydraulic Engineering, Delft University of Technology, Delft, The Netherlands, [3]Deltares, Delft, The Netherlands, [4]Now at Water Safety Policy Advisor, Personal capacity, The Hague, The Netherlands, [5]Department of Hydraulic Engineering, Delft University of Technology, Delft, The Netherlands, [6]Faculty of Civil Engineering and Geosciences, Delft University of Technology, Delft, The Netherlands

Key Points:

- Characterizing the effect of groynes on river flow in two-dimensional hydrodynamic models by using weir formulas was evaluated
- Alternative methods to implement groynes into two- and three-dimensional river models were proposed, and their reliability was tested
- The performances of two of the available modeling options in simulating the groyne modifications were assessed

Supporting Information:

Supporting Information may be found in the online version of this article.

Correspondence to:

B. Yildiz,
burhanyildiz@mu.edu.tr

Citation:

Yildiz, B., Ambagts, L., Yossef, M. F. M., & Mosselman, E. (2024). Evaluation of different numerical approaches to modeling flood flows over groynes. *Water Resources Research*, *60*, e2023WR036895. https://doi.org/10.1029/2023WR036895

Received 15 DEC 2023
Accepted 24 MAY 2024

Author Contributions:

Conceptualization: Burhan Yildiz, Lindert Ambagts, Mohamed F. M. Yossef, Erik Mosselman
Data curation: Lindert Ambagts
Formal analysis: Lindert Ambagts
Investigation: Burhan Yildiz, Lindert Ambagts
Methodology: Burhan Yildiz, Lindert Ambagts, Mohamed F. M. Yossef, Erik Mosselman
Resources: Lindert Ambagts
Supervision: Mohamed F. M. Yossef, Erik Mosselman
Validation: Lindert Ambagts
Visualization: Lindert Ambagts
Writing – original draft: Burhan Yildiz, Lindert Ambagts

Abstract The hydraulic resistance of groynes is an important factor in the determination of design flood water levels on rivers and the assessment of how much these levels are lowered by modifying the groynes. In standard one- or two-dimensional numerical hydrodynamic models for flood risk management, groynes are commonly represented as subgrid features with a local energy loss according to a weir formula. We tested this representation by using a two-dimensional horizontal mesh at various groyne submergence degrees by comparing the results with those of flume experiments. We also compared the results with simulations using different 2D and 3D approaches on finer grids that incorporate groynes in the bed topography. In one of the two tested 3D models, complete Reynolds-averaged Navier-Stokes equations were solved. The second tested 3D model was constructed simpler by assuming hydrostatic pressure distribution in the vertical direction. We employed Delft3D software in construction and execution of all models. One of the 3D models did predict the hydraulic resistance at low submergence better than the standard model, but it slightly underestimated the resistance at higher submergences. Despite differences in flow characteristics, weirs and groynes were found to produce similar flow resistances for the same height and boundary conditions. Simulations of groyne modifications showed that hydraulic resistance decreased nonlinearly with groyne lowering and streamlining.

Plain Language Summary Groynes are used for river training. Their positive effects include riverbank stabilization, improvement of navigability and prevention of ice jams. However, during floods they become submerged and increase the flood water depths by blocking the flow and increasing turbulence. This may lead to severe outcomes. Floods are among the most fatal disasters that affect the globe. Even an increase of flood water depths by some centimeters may cause disastrous outcomes. Engineers generally resort to approximate solutions for adding the effects of groynes into hydraulic flood models for long river reaches. In this paper, we assess the capabilities of these approximate models as well as those of more simplified and more advanced models. Insights were sought to help flood modelers for better prediction of flood water levels. Our study shows that the most widely used groyne resistance model leaves room for further development, despite demonstrated capabilities.

1. Introduction

Many lowland rivers around the world have been embanked to protect the surrounding land against flooding. Urban and agricultural developments often encroached onto the floodplains, deteriorating riparian nature, increasing flood water levels and, hence, necessitating raising of the embankments. Increasing value of the protected land due to population growth and economic development prompted even further raising of the embankments. Objections by ecologists and protests against the demolition of houses and degradation of landscapes for dike reinforcements paved the way for a different approach in the Netherlands, based on giving more space to the river instead of continuing to raise dikes. This approach was not immediately embraced but eventually resulted in the Room-for-the-River program, thanks to media attention and shocks in public opinion by the floods of 1993 and 1995 (Mosselman, 2022). It was realized that giving more space also made the flood defenses more robust in the face of increased uncertainties in future design flood conditions due to climate change (Klijn et al., 2018). Meanwhile many lowland rivers also underwent another form of engineering. Their main channels were trained with groynes, like in the Rhine branches in the Netherlands and Germany, the Mississippi and Missouri rivers in the United States, and the Danube in Austria. Groynes were initially applied locally to protect

Writing – review & editing: Burhan Yildiz, Mohamed F. M. Yossef, Erik Mosselman

riverbanks against erosion, but eventually systematically along long river reaches to prevent ice jamming and to improve navigability (Yossef, 2005). Groynes provide additional flow resistance and constrict the main channel. At low flows this is favorable as they increase the navigable depth in the main channel. At high flows, however, these effects raise the flood water levels. Moreover, river training has set off a process of riverbed erosion, rendering the relative elevation of groynes above the riverbed unnecessarily high (Havinga, 2020; Mosselman, 2022). This increases their hydraulic resistance and raises flood water levels. Reducing this resistance by lowering or streamlining groynes has thus become a key measure of Room for the River in the Netherlands (Rijkswaterstaat, n.d.), as well as an important issue elsewhere (Huthoff et al., 2013). This underscores the great importance of the hydraulic resistance of groynes. The effects of submerged groynes on flow, however, has been researched much less than the effects of emerged groynes (e.g., Jeon et al., 2018; Kang et al., 2016; Koken & Constantinescu, 2011). The numerical representation of the hydraulic resistance of groynes at varying water levels remains subject to debate. In 1D (one-dimensional) and 2DH (two-dimensional horizontal) numerical models, groynes are commonly represented as subgrid features with a local energy loss according to a submerged-weir discharge formula (Ali, 2013; Bloemberg, 2001; Jongeling et al., 2010; Mosselman & Struiksma, 1992; van Broekhoven, 2007; Yossef, 2005, 2017; Yossef & de Vriend, 2011; Zagonjolli et al., 2017). The problem is that flow over groynes differs from flow over weirs. Part of the flow bypasses groynes and energy is also lost in the mixing layer that develops downstream of the groyne head. The weirs on the other hand cover the whole width of the channel and work as a control structure. This is accounted for by adapting the submerged-weir discharge formulas. However, proper simulation of water depths at high submergence rates remains a problem. The details of this issue are provided in the next section.

Numerical modeling of flow over and around groynes has been conducted for other purposes as well. Tritthart et al. (2009) used numerical modeling to simulate flow in a groyne field along a branch of the Danube River focusing on natural habitat conservation. They used a 3D (three-dimensional) RANS (Reynolds-averaged Navier-Stokes) model with grid spacing changing between 3 and 8 m in the mesh and k-ε turbulence closure. Glock et al. (2017) and Glas et al. (2018) used the same solver for modeling flow hydrodynamics and morphology changes in the groyne field and the main channel. Kashyap et al. (2010) simulated submerged-groyne flow at a bend flume using an LES (large-eddy simulation) numerical model. They focused on the flow characteristics and bed shear stresses at one submergence level considering scour. Xiang et al. (2020) used LES to simulate flow at a groyne field with vegetation. Both numerical models were validated with flume experiments. They used fine meshes as required by LES however they are unfeasible in practical river modeling applications with long reaches.

Groyne lowering was one of the measures in the Room-for-the-River program. Streamlining of groynes had been proposed too (Havinga, 2020; van Stokkom et al., 2005). The effects had to be assessed using numerical models. This implies that the numerical models to simulate groyne flow should work well for design flood conditions and various groyne geometries. However, existing literature does not contain many studies related to submerged groynes and does not offer information on the effect of groyne modifications on flow resistance and flood water levels. In this study, our first objective is to test how reliable the standard numerical models of common flood risk management practice are in estimating the resistance of submerged groynes. For that we compare standard model results with experimental recordings. Our second objective is to assess the potential improvements from computationally more expensive modeling approaches, testing their results against the same experimental data. Finally, our third objective is to evaluate the performance of the different modeling approaches in simulating the effects of groyne modifications such as lowering and streamlining. In the absence of experimental data, this evaluation is based on intercomparison of model results.

2. Modeling of Groynes in Depth-Averaged Models

The effects of interventions on flood water levels in the Netherlands are generally assessed using 2DH numerical models which solve the shallow-water equations. These equations result from integrating the RANS equations over depth, assuming the horizontal length scales of interest to be much larger than the vertical length scale. This shallow-water approximation is valid for rivers that are sufficiently wide to exclude influences from near-bank vertical flows on the central flow field. The cells of the computational grids can be about 40 m long and 20 m wide. However, these grids are not fine enough to accurately represent the geometry of groynes that are generally 20–200 m long and 5–10 m wide. Therefore, groynes are represented by subgrid parameterizations for the corresponding energy losses.

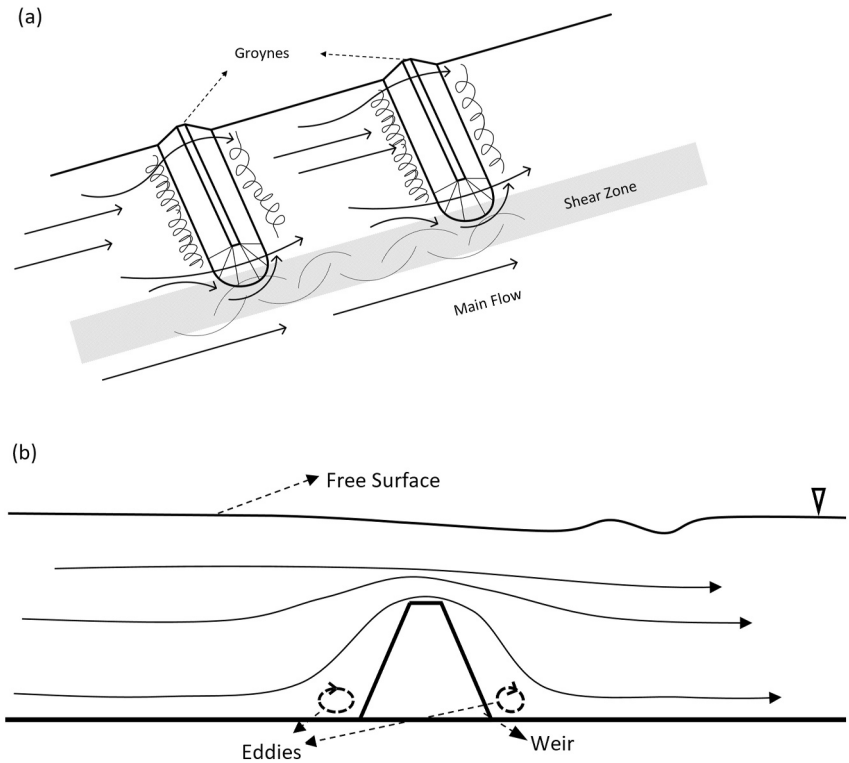

Figure 1. (a) Three dimensional flow field over submerged groynes without a flood plain. Solid lines with arrows correspond to the streamlines, curves with gray background correspond to the shear zone and swirling lines before and after the groynes correspond to the eddies. (b) Two-dimensional flow field over a submerged broad crested weir plotted at a vertical plane. Solid lines with arrows correspond to streamlines, circular dashes correspond to possible forming eddies depending on the upstream and downstream face slopes of the weir.

The effects of groynes are parameterized by defining them as weirs and assigning a representative weir coefficient (Mosselman & Struiksma, 1992). A submerged weir differs from a weir with modular flow, because it is affected by the water level downstream. Modular weir flow, not affected by the water level downstream, has been analyzed extensively, resulting in reliable empirical equations (Bos, 1989; Chanson, 2004; Fritz & Hager, 1998; Hager & Schwalt, 1994). For a submerged weir, the effect of the downstream water level is accounted for by a discharge reduction function (φ) which depends on submergence S, where $S = H_2/H_1$ with H_2 downstream flow depth and H_1 upstream flow depth (Villemonte, 1947). It is generally formulated as (Ali, 2013):

$$\varphi = \sqrt{1 - S^P} \tag{1}$$

where P is a fit parameter based on the experimental data and considering the geometric effects of the weir. At high submergence levels, common during floods, φ is sensitive to the fit parameter P. One might think that this could be reduced by model calibration, but in practice the limited available point measurements lead to a problem of equifinality (Williams et al., 2020). Multiple combinations of parameter settings can yield the same results. This maintains uncertainty in extrapolation to extreme flood events or assessment of the effects of groyne modifications.

The flow over submerged groynes differs fundamentally from submerged-weir flow. While the weir acts as a control structure covering the whole width of the channel, the groyne region is connected to the main channel, allowing lateral exchange of momentum and creating shear zones due to the velocity differences between the two flow fields that arise from flow separation at the tip of the groyne (Figure 1). These shear zones form mixing layers in the transition area between the main channel and the groyne field. Yossef and de Vriend (2011) show that the mixing layer extends in the flow direction with almost the same intensity when there is a series of groynes. This transfers momentum from the main channel to the groynes region. Such a mixing layer in the horizontal

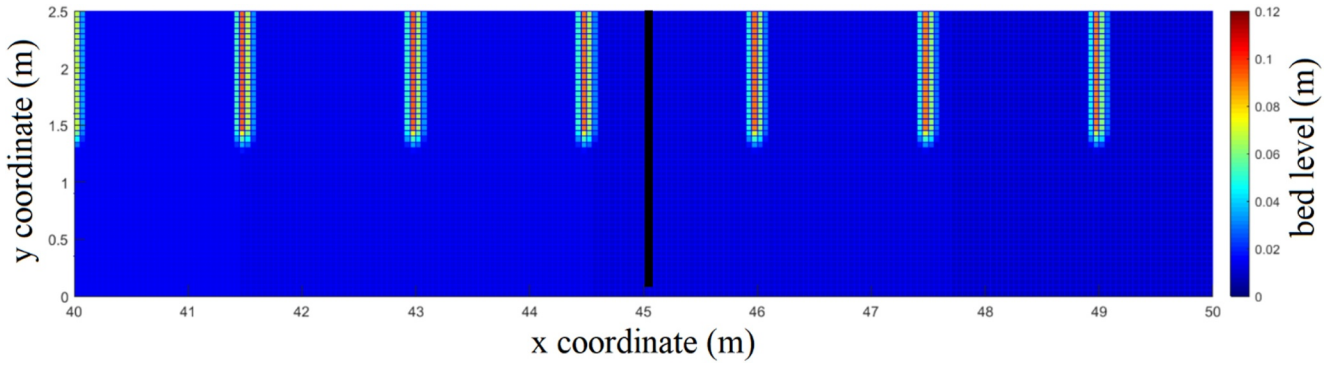

Figure 2. Top view of the mesh generated for simulations 2DH-F, 3DH and 3D (see Table 2) (black line corresponds to the depth averaged velocity profile measurement section at Figure 7) (flow direction is from left to right).

plane is not formed at weirs as weirs block the entire flow width. In submerged-weir flow, energy is mainly lost through flow impingement on the bed along with vertical flow contraction and separation with formation of a vertical eddy at the lee side of the weir. A similar vertical eddy may also form in the groyne flow, but lateral momentum transfer from the main channel flow to the groyne field decreases the underpressure around the groyne crest and in the eddy, thus weakening the eddy and the flow impingement. This results in less shear, less curved streamlines and smaller energy losses (Jongeling et al., 2010; Mosselman, 2018). These effects are expected near the groyne head whereas further away from the groyne head the flow over a groyne may resemble more the flow over a weir, especially if groynes are long.

As an alternative to defining them as subgrid elements, groynes can be incorporated in the bed topography. This method needs finer meshes which would increase the computational cost. Nonetheless, we also tested this as an alternative to the standard approach. It is worth noting that morphodynamic changes of the river bed around groynes during floods render the prediction of the hydraulic resistance of groynes even more complicated.

3. Methodology

We developed numerical models for the same flume, groyne and inflow conditions as in the laboratory experiments conducted by the Bundesanstalt für Wasserbau (BAW) in Karlsruhe in 2011 (Hüsener, 2015; Hüsener et al., 2012). Their laboratory flume was 75 m long and 2.5 m wide. They conducted experiments without groynes and with groynes spaced 1.5 m apart (Figure 2). They recorded the water surface levels throughout the flume by using a three-camera particle tracking (PTV) approach and at some specific locations by using ultrasonic sensors for validation. The velocities were recorded by using the PTV and Acoustic Doppler Velocimetry (ADV) method. For reference, we prepared a series of cases without groynes (V00). For the tests with groynes (V01), we represented the groynes by two approaches. In the standard model, we implemented the groynes as subgrid weirs. In the remaining models, we implemented them in the bed topography as done in the experiments with 80 mm height, 1V:1H upstream slope and 1V:1.5H downstream slope. The groyne length was 1 m with an additional 0.2 m length toe portion leading to a 1V:2.5H lateral slope. We used the same stage-discharge relations as in the experiments to allow comparison (Table 1). The case names were assigned indicating the flow depths in them (i.e., h70 for case having 70 mm flow depth). For the largest discharge tested, the water column above the groynes was 12–14 cm. As this is 50%–75% higher than the 8 cm high groynes themselves, we consider the model results pertinent to design flood conditions. While our main attention regards the submerged groyne cases, we also modeled two emerged-groyne cases. The results of the emerged cases are not documented here in detail, but they were used in the calibration phase. The experimental data of Hüsener et al. (2012) and Hüsener (2015) include discharge, water level and velocity field measurements and are presented in more detail by Ambagts (2019).

Table 1
Flow Conditions in Numerical Models (After Hüsener et al., 2012) (The Cases Which Were Used in Calibrations Were Labeled With an Asterisk)

Case	h70	h80	h100	h120	h160	h200
Water depth (mm)	70	80	100	120	160	200
Discharge V00 (l/s)	42*	52*	74.5*	100*	157.8*	222*
Discharge V01 (l/s)	21	26	40.5*	56*	92	128

We used Delft3D software for setting up and simulating the cases. It has a long track record of application and validation (Duc et al., 2004; Gerritsen et al., 2008; Mosselman, 2004). Delft3D uses a finite-volume method for the

Table 2
Numerical Model Properties

Simulation type	Grid	Grid size: x, y, z (m)			Groyne representation	Model code
2D horizontal	Coarse	0.25	0.25		Subgrid weir	2DH-C
2D horizontal	Fine	0.05	0.05		Bed topography	2DH-F
3D hydrostatic	Fine	0.05	0.05	0.01	Bed topography	3D-H
3D non-hydrostatic	Fine	0.05	0.05	0.01	Bed topography	3D-NH
2D vertical	Fine	0.05		0.01	Bed topography (Weir)	2DV-F

numerical solution of the flow equations (Deltares, 2014). Continuity and RANS equations are integrated over volume and time at the discretized control volumes. Model equations are provided in the Supporting Text S1. For the transient terms, the Crank-Nicolson method is used for discretization which is implicit. Its Taylor series truncation error is second order. The spatial discretization is achieved by using the Cyclic method (Stelling & Leendertse, 1992). This method includes a third-order upwind scheme and central differentiating. This makes the accuracy for the spatial terms also second order. To eliminate the possible overshoots or undershoots due to the usage of higher-order differentiating schemes, a Forester filter is used to remove the computational noise (Forester, 1977). The turbulent stresses are estimated using the eddy viscosity approach. This method is closed with a standard k-ε turbulence model (Launder & Spalding, 1974) which defines eddy viscosity using k (turbulence kinetic energy) and ε (rate of viscous dissipation). Two additional transport equations are written for them. A staggered grid is used by defining velocity values at the cell faces and pressure values at the cell centers to eliminate pressure oscillations. We used structured meshes without any local refinements in each model to allow better comparison between their results.

We constructed four models to simulate the experiments: 2DH-C, 2DH-F, 3D-H, 3D-NH, and one model to simulate weir flow: 2DV-F (Table 2) such that the results could be used to compare the weir flow and groyne flow. 2DH-C (two-dimensional horizontal with coarse mesh) is the standard 2D model that uses a coarse horizontal mesh (25–25 cm) and shallow-water equations which result from integrating the RANS equations over depth. We approximated the common flood risk management practice and used 10 computational cells in lateral direction and the same cell length in the flow direction. The meshes selected in the other models were finer than this mesh. Therefore, we labeled this mesh as coarse. The groynes were defined as subgrid weirs. The eddy viscosity was anisotropic in the shallow-water equations, assuming most of the turbulence in the flow was generated in the horizontal direction. The method of turbulence closure is of minor importance at the subgrid weir formulation as flow separation and mixing layer formation are not explicitly modeled there. 2DH-F (2D horizontal with fine mesh) is again a 2D horizontal model, but with a finer mesh (5 cm × 5 cm). It allows inclusion of groyne geometry in the bed topography. Therefore, no sub-grid weir formulation was used here. The 3D-H (three-dimensional hydrostatic) model has a three-dimensional mesh, but the RANS equations are solved only in the two horizontal directions. The vertical RANS equation is simplified into a hydrostatic pressure equation. In the 3D-NH (3D non-hydrostatic) model, RANS equations are solved in all three directions. In the meshes generated for 3D models the groynes were defined as a part of the bed topography. The cell sizes are provided at Table 2.

In each of these models, the outlet and inlet boundary conditions were water levels and water discharges, respectively, while the upstream water levels were predicted. Furthermore, one two-dimensional vertical model, namely 2DV-F (two-dimensional vertical with fine mesh), was constructed to model weir flow. The model had 0.05 m grid size in x and 0.01 m grid size in z direction. The aim of constructing this model was to compare the weir and groyne flows under the same upstream and downstream boundary conditions.

We calibrated the numerical models in this study on detailed data from flume experiments. Calibration on data from a real river might have been preferred, but it would be hard to obtain measurement data with the same level of detail. The models were calibrated first on V00 cases without groynes by modifying the bed and side roughness values of the flume to match the simulated water levels to the corresponding experimental results. We used four flow depths of the submerged cases (h = 100, 120, 160 and 200 mm) in this calibration. Then, the obtained values were employed with the groynes to calibrate the models at V01 cases with groynes. We modified the background horizontal eddy viscosity term at the emerged and submerged cases to calibrate the water levels. Background horizontal eddy viscosity is defined in Delft3D and works as a calibration term. Additionally, the groyne face

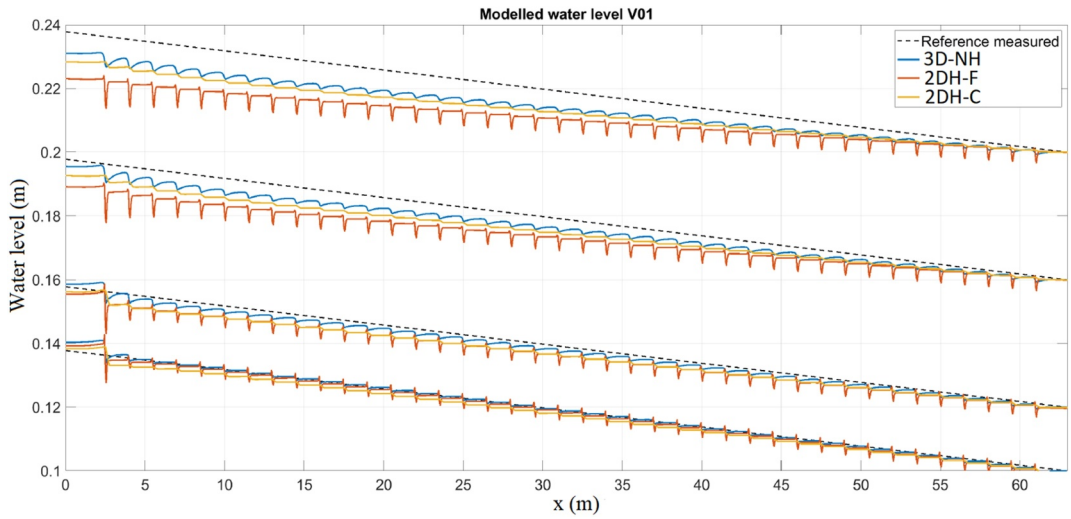

Figure 3. Comparison of measured and modeled water levels for various models and upstream flow depths (from top to bottom: h200, h160, h120, h100).

roughness was modified using the velocity field around the groynes. Later, we modeled groyne modifications by using 2DH-C and 3D-NH models. We selected three heights of lowering that corresponded to 12.5%, 25% and 37.5% of the original height. We streamlined groynes by flattening the downstream slope of each groyne from 1V:1.5H to 1V:5H and 1V:10H.

4. Results and Discussion

In this section, we focus on the water levels as they reflect the overall flow resistance added by the groynes. We then use velocity field predictions at selected flow sections to further assess the strengths and weaknesses of each model. This section is divided into six subsections covering the results and discussion of the following topics: (a) calibration of the models, (b) performance of the 3D models at varying submergence rates, (c) performance of the 2D models at varying submergence rates, (d) comparison of submerged weir and groyne flows, (e) the effects of groyne modifications on water levels and (f) the projection of the results on real rivers.

4.1. Model Calibrations

The first set of calibrations was applied to V00 cases, yielding roughness values. Nikuradse bottom roughness of 7.5 mm at the bottom and 0.2 mm at the sides were obtained in 2DH models when using the fine mesh, whereas these values were obtained as 10 and 0.33 mm, respectively, for 3D models. At moderate to high flow depths (h100, h120, h160 and h200), the models predicted the water levels well with a maximum water surface slope percentage error of 3.5% which we found acceptable. For V01 cases, the surface roughness values on the groynes were altered as the groyne surfaces were constructed as smooth in the experiments. This calibration using the ADV recordings over the groynes resulted in a roughness height equal to 1 mm at the groyne surface. Then, the background horizontal eddy viscosity terms were modified to predict the water surface profiles at moderate depths (h100, h120). The results after the second set of calibrations of V01 cases are given in Figure 3 for models 3D-NH, 2DH-F and 2DH-C. The results of 3D-H were close to the results of 3D-NH. All models could be calibrated well at low-water levels up to h120. The 2DH-F model had the largest deviation from the experimental results at high water levels. The water levels fluctuated most at the first groyne crossings, because of the unproportioned discharge distribution at the flume entrance. These fluctuations were dampened in the other groyne crossings.

In the experimental study, the discharges at the main channel and the groyne crossings were calculated by using ADV recordings. This was achieved only in the h160 case. In the models, the boundaries of the main channel and the groyne field were used as they were defined in the experimental study: $0 < y < 1.5$ m corresponds to main channel, 1.5 m $< y <$ 2.5 m corresponds to groyne field (see Figure 2). By using the model results, the percent of

Table 3
Comparison of Measured and Modeled Discharge Percentages Passing Through the Groyne Field at h160

Model/Measurement	%Q passing through the groyne field	Deviation (%)
Measured	15.3	–
2DH-C	28.6	13.3
2DH-F	23.1	7.8
3D-H	18.4	3.1
3D-NH	16.7	1.4

discharge passing through the groyne field was estimated at h160. The results are given in Table 3. The 3D-NH model predicted closest to the experiments with 1.4% deviation. Then followed 3D-H, 2DH-F and 2DH-C.

4.2. 3D Models

In 3D models, the groynes were only defined in the bed topography by using a mesh that gives the possibility. The 3D-H and 3D-NH models performed closely in discharge distribution prediction between the main channel and the groyne field and the water level predictions. The biggest deviation at the computed water levels were around 3% of the measured depth at the entrance of the flume for the case with the highest submergence (h200). Figure 4 shows water level and surface velocity predictions of these two models at an uncalibrated case (h160) along with the measured data. At the top figure, the vertical axis scale covers a small range to visualize the smallest changes in the free surface. Groyne crests are outside this range, far below the plotted levels. The 3D-H model reduces the vertical momentum equation to a hydrostatic pressure equation. This eliminates formation of negative pressure zones over the crest and leads to more acceleration of flow while approaching the groyne. The associated energy losses make the water level in the 3D-H model drop more steeply at the groyne and recover faster at the lee side, whereas the water level profile is smoother in the 3D-NH model, closer to the actual behavior. The lowest water elevation was observed just over the crest at the numerical models; however it was measured around two-groyne-heights distance downstream from the groynes at the experiments. This also changes the location of the maximum streamwise velocity between the models and the measurement. This can be observed at the bottom panel of Figure 4. The location of measured maximum velocity coincides with the location of the lowest water level. This location indicates where the streamlines are horizontal before turning downward. This indicates that the vertical eddy is as high as the groyne in the model. However, it was larger in the experiments. Larger eddies do not only dissipate more energy of the flow; they also reduce the flow section, producing larger flow velocities, accelerations and decelerations and hence larger energy losses. The 3D-NH model predicted the surface velocities better than the 3D-H model. However, the measured minimum velocities were generally below the modeled ones. This means that neither of the two models reproduced the losses associated with the decelerations well. The measured velocity extremes were observed for some distance in the groyne field. Although the 3D-NH model predicts this behavior better than the 3D-H model, peak velocities developed more rapidly in both models than in the laboratory experiments. This also led to smaller energy losses in the simulations. Figure 5 shows 3D-NH and 3D-H model output of the streamwise velocity contours with the velocity vectors. A vertical recirculation zone is visible at the lee side of the groynes. Its streamwise length decreases with increasing flow depth over the groyne. The

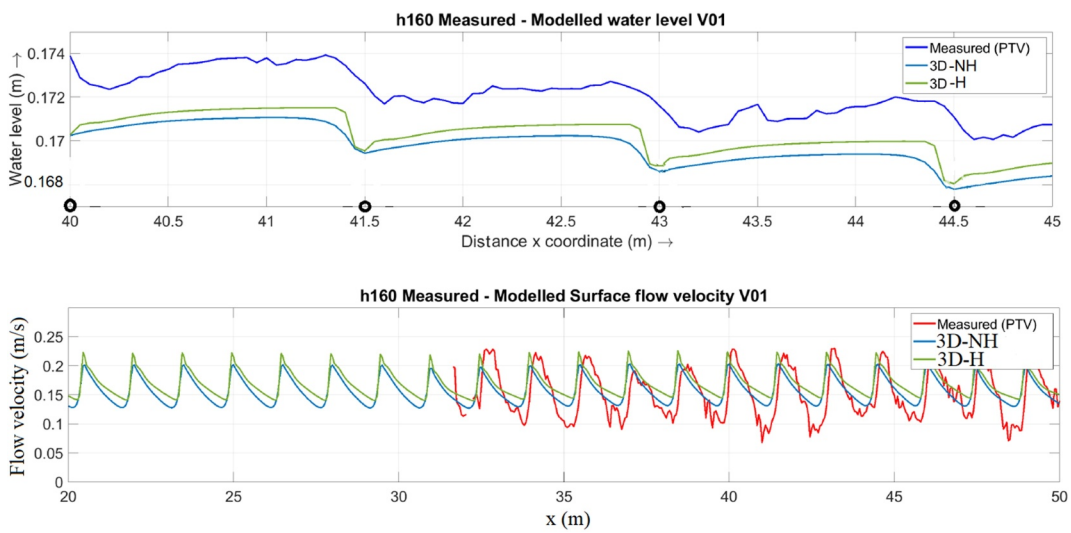

Figure 4. Measured and modeled (with 3D-NH and 3D-H) water levels (top) and surface velocities (bottom) at $y = 2.25$ m for case h160. x-coordinates of the groyne locations are labeled with circles.

10.1029/2023WR036895

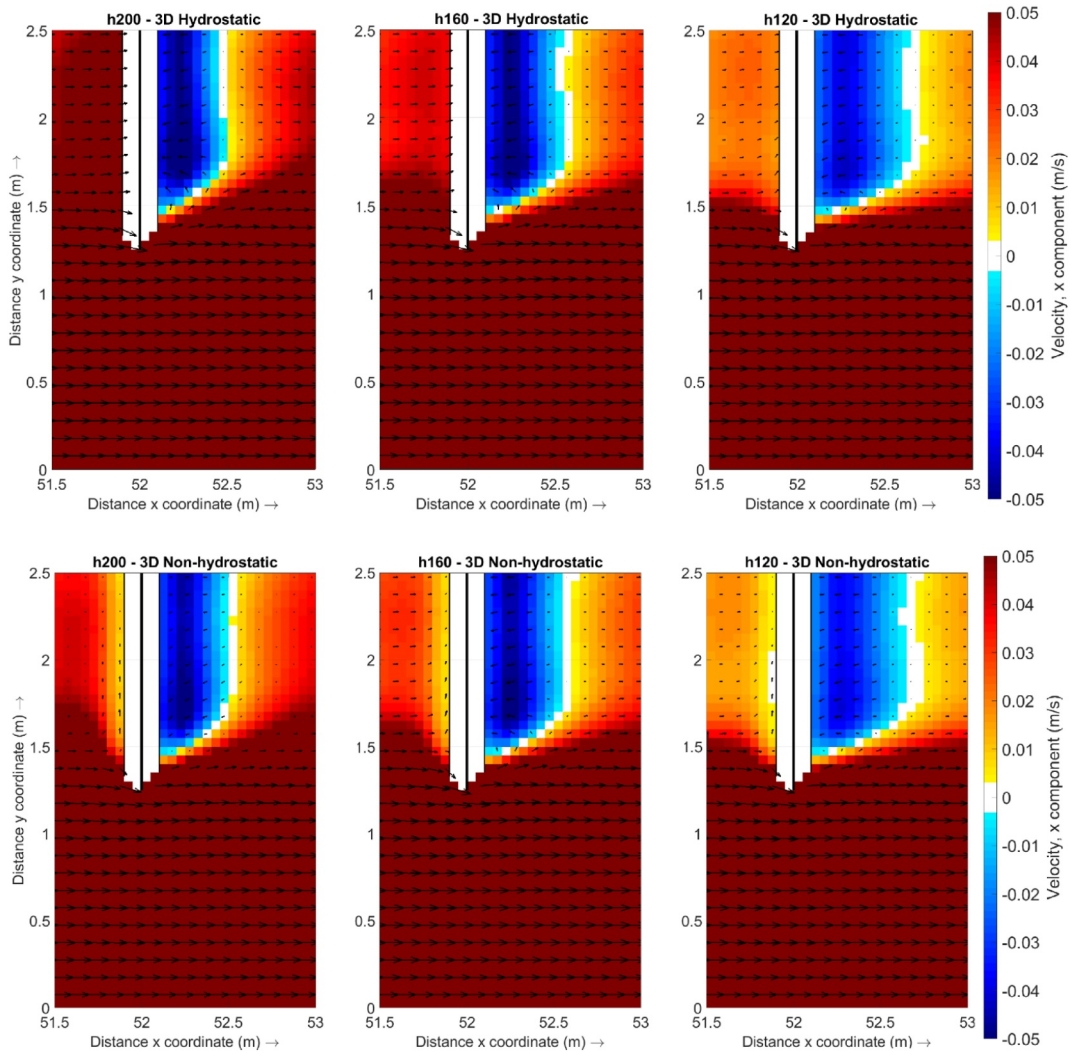

Figure 5. Streamwise velocity contours with the velocity vectors just above the bed.

flow reattaches closer to the groyne in the 3D-H than in the 3D-NH model. This is because the flow decelerates less in the groyne fields in the hydrostatic model, thereby underestimating the energy losses and increasing the discharge through the groyne fields. The higher flow velocities lead to the flow reattaching closer to the groyne. The results of the 3D-NH model are compatible with the experimental data. The errors in predicting the eddy size might be related to the selection of the turbulence closure method in the RANS model. The k-ε turbulence closure is known to have limitations in simulating flow separation (Rodi, 2017; Tritthart et al., 2009). Besides, the mesh resolution used at this stage could explain the systematic deviation of the results from the measurements when the submergence rate increases further away from the calibrated cases. Finer meshes could be used to solve this problem, but river engineering applications to long river reaches would become computationally expensive and impractical.

4.3. 2D Models

The number of the computational cells needed for 2DH-F and 2DH-C models was only 75,000 and 3,000, respectively, which was much smaller than the ones of the 3D models (more than $2{\cdot}10^6$). Therefore, the 2D models required much less time than the 3D models. The 2DH-F model results deviated more than the 2DH-C model results from the experimental recordings at the uncalibrated cases. The maximum modeled water level deviation from the measured one is around 4% at the 2DH-C, while it is 6% at the 2DH-F model. Both models gave the biggest deviations at the entrance of the flume for the case with the highest submergence (h200). 2DH-F

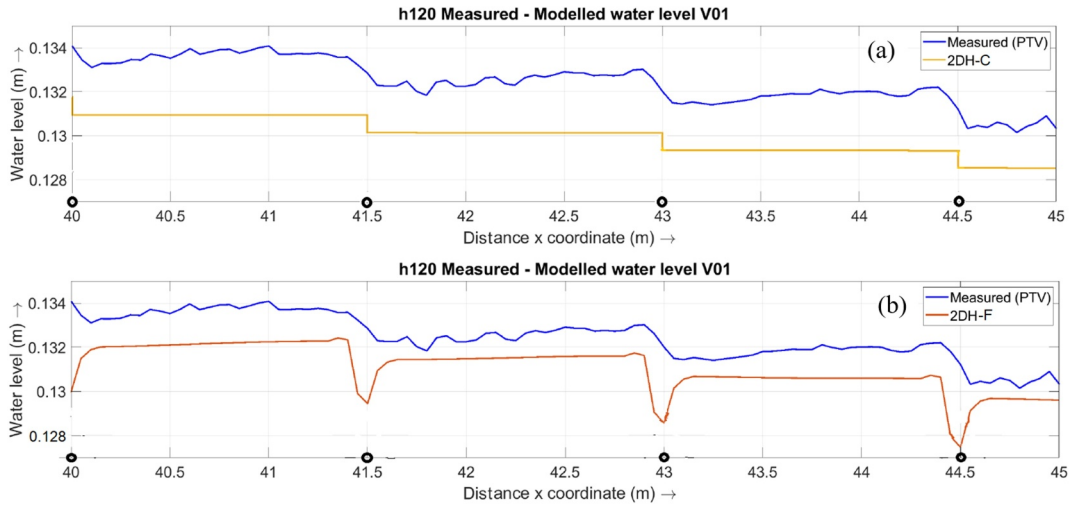

Figure 6. Water level profiles from (a) 2DH-C (b) 2DH-F models at $y = 2.25$ m. x-coordinates of the groyne locations are labeled with circles.

does not include vertical accelerations and cannot solve for vertical eddies. Therefore, energy losses in this model can only be ascribed to lateral momentum exchange and acceleration-deceleration losses from the depth-averaged velocities. The 2DH-C model uses the subgrid weir representation of groynes. It also underestimates energy losses at high submergence values. This leads to more discharge over the groyne fields, less discharge through the main channel and accordingly smaller velocity gradients in the mixing layer between the groyne field and the main channel.

Figure 6 shows the comparison between measured and modeled water levels for the 2DH-F and 2DH-C models in the h120 case between x = 40 and 45 m. With the same reason of Figure 4 (top), the vertical axis scale covers a small range and the groyne crests are outside this range. In the 2DH-F model, the drop is prominent with an instant rise behind the groyne. The water level is almost horizontal between two groyne surroundings. In the 2DH-C model, the drop occurs at the groyne location only whereas beyond that location the water surface is almost horizontal as the resistance there is associated with the bed friction only which is small. The differences between models comply with expectations. The 2DH-F model does not resolve vertical flow accelerations. The deceleration and acceleration losses around the groyne in the horizontal plane dominate the other loss terms, which is not reproduced by the mere head loss of the subgrid representation of the 2DH-C model.

The depth averaged flow x-velocity values of 2DH-C model gave comparable results with the 3D-NH model. Figure 7 shows a comparison for one emerged (h70) and one submerged (h160) case at a lateral section taken at the middle of a groyne field ($x = 45.25$ m location). Although the 3D-NH and 2DH-C models solve for the 3D RANS and the shallow water equations respectively, their results are similar at most parts of the channel width. However, the flow resistance does not only depend on the mean velocity values but also depends on the gradients of velocities. Therefore, this fit between the 3D-NH and 2DH-C model does not guarantee the same flow resistance to be seen in both models, which was also demonstrated in water level curves.

4.4. Comparison Between Submerged Weir and Submerged Groyne Flows

The 2DV-F model was constructed to simulate a full-width weir flow with the same grid size in x- and z-directions as in 3D models. The inflow discharge is defined as unit discharge as measured from the groyne model over the crest. This allows direct comparison of the weir and groyne flows. Figure 8 shows streamwise velocity contours and vectors of both 2DV-F and 3D-NH models. The transect across the groyne was taken inside the groyne field. The 2DV-F model resolved the velocity profile above the crest similarly as the 3D-NH model. The streamwise length of the vertical recirculation zones are almost the same in the two models. Figure 9 shows that the water levels from both models match closely with a maximum of 2 mm difference at the first groynes or weirs for the h120 case, which is the calibrated case. At h160 and h200 cases, both results remain close to each other. The

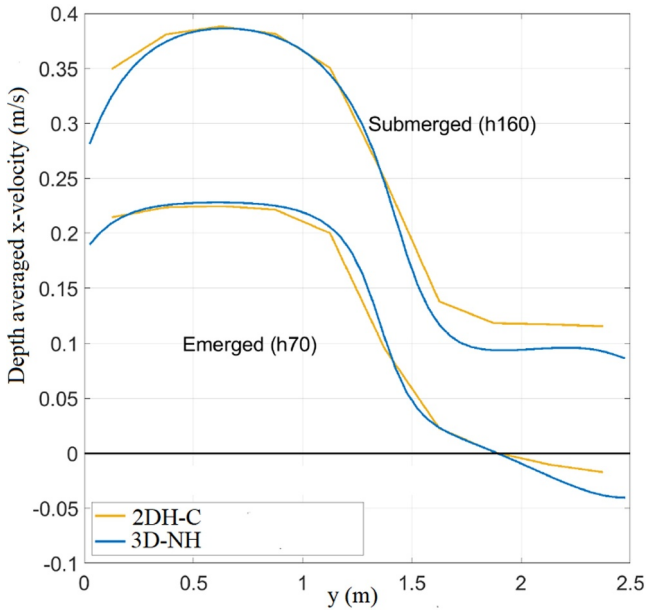

Figure 7. Comparison of depth-averaged flow velocities at the middle of the groyne field at $x = 45.25$ m. (The location of the section in the flume is shown in Figure 2).

difference at the first structures can be explained from the length needed to develop the proper discharge distribution between main channel and groyne field in the 3D model, which is not the case in the 2DV-F model.

4.5. Effects of Groyne Modifications on Water Levels

We selected the 3D-NH model to assess the effects of groyne modifications as it outperformed the other models. Additionally, the 2DH-C model was used to assess the performance of the standard model in practice. We used both models for groyne lowering but only the 3D-NH model for groyne streamlining as this modification was not possible in the 2DH-C model. The results of the simulations are given in Figure 10. For 1 cm of groyne lowering, the 2DH-C model predicted an 8 mm drop of the upstream water level at case h100 whereas the 3D-NH model predicted a drop of only 2 mm. For higher submergence, however, the drop in water level decreased as the lowering amount becomes relatively small compared to the flow depth and the results from both models became closer. The first and second centimeter of lowering are more effective than an additional lowering from 2 to 3 cm. The discharge and flow velocities were larger over lower groynes owing to the resulting larger cross-sections.

The original downstream slope of the groyne geometry (1V:1.5H) was streamlined to the slopes 1V:5H and 1V:10H to see the effect of this modification on water levels. The maximum drop at the inlet water levels was 3.5 mm at h200 when the groyne slopes were streamlined to 1V:10H. At high submergences, the decrease enlarged for both the 1V:5H and 1V:10H cases. The changes were largest in the h120 to h160 cases. When the streamlining increased from 1V:5H to 1V:10H, the water level decline improved by around 20% at each submergence rate. Bloemberg (2001) states for slopes smaller than 1V:8H that the flow separation disappears and that energy losses thus decrease considerably. This is confirmed by a 3D model simulation for a 1V:10H slope where no recirculating eddy is observed at the downstream side (Figure 11). Therefore, the degree of water level drop decreased at the 1V:5H to 1V:10H transition, compared to the transition from 1V:1.5H to 1V:5H.

4.6. Projection of the Results on Real Rivers

The flume dimensions used in this study are much smaller than those of real rivers. The experimental setup differs too, because it does not contain a flood plain which affects the flow structures. The groynes in the setup cover almost half of the flume width, whereas in reality groynes make up a smaller fraction of the river cross-section.

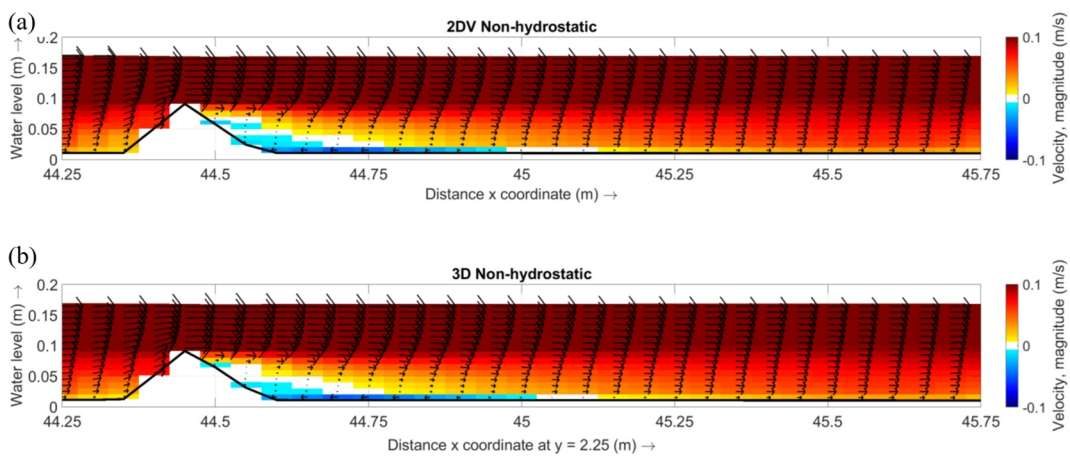

Figure 8. Streamwise velocity contours and vectors at a longitudinal section for case h160 from (a) 2DV-F model (weir model) (b) 3D model over the groyne at $y = 2.25$ m (groyne model).

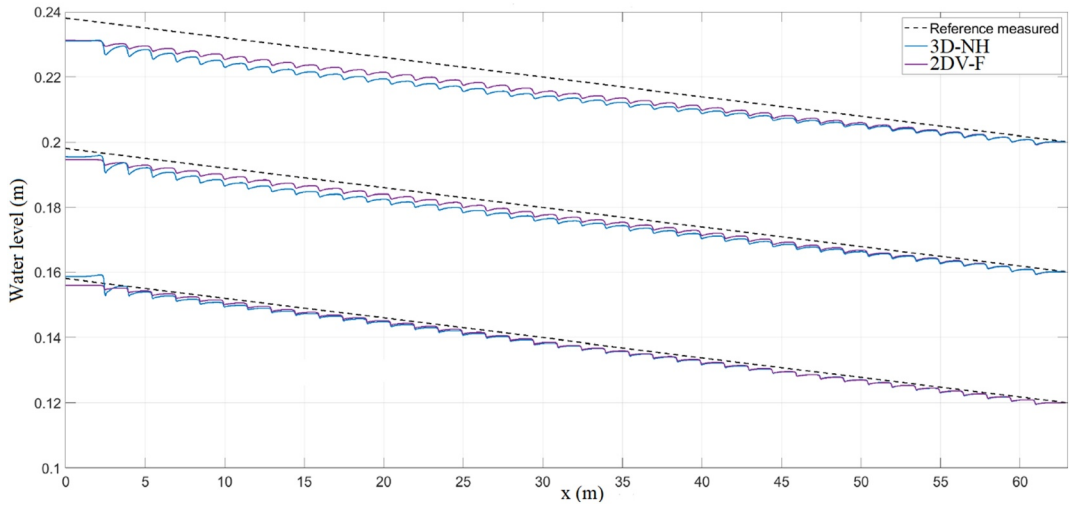

Figure 9. 2DV-F and 3D model results of water levels over groynes and weirs with the experimental result for three cases (h120, h160 and h200).

This can inflate the relative resistance of groynes and overestimate the effect of groyne modifications. Furthermore, field observations suggest that changes in riverbed morphology during floods can make groyne resistance in real rivers smaller than assumed in numerical models. By trapping and depositing sand at the lee side, groynes assume a more streamlined shape with less flow resistance, as shown in Figure 12. Practicing engineers or researchers should consider these aspects when using the outcomes of this study.

5. Conclusions

We tested four modeling approaches to simulate flow over groynes at different degrees of submergence and used two of them to simulate the flow at varying groyne geometry. We selected these models among the ones that could be applied to the models of rivers with kilometers of reach lengths. Therefore, it was expected that each approach would have strengths and weaknesses at varying conditions. In the standard approach, groynes were represented as a subgrid contribution to hydraulic resistance by a weir formula in depth-averaged (2DH) models. We incorporated them in the bed topography in 2DH, 3D hydrostatic and 3D non-hydrostatic models using finer

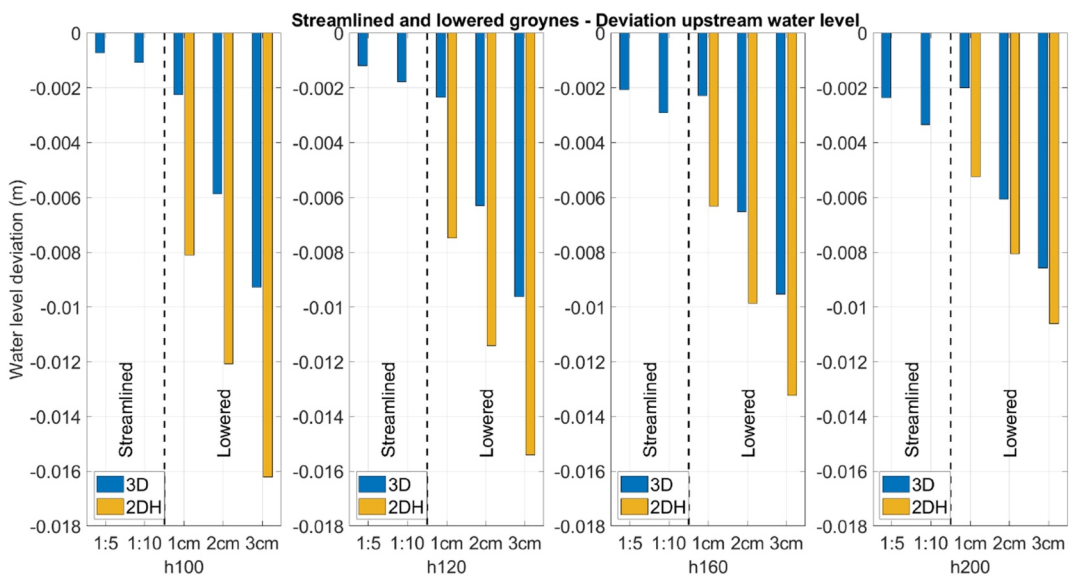

Figure 10. Upstream water level drop after groyne lowering or streamlining at various submergence rates.

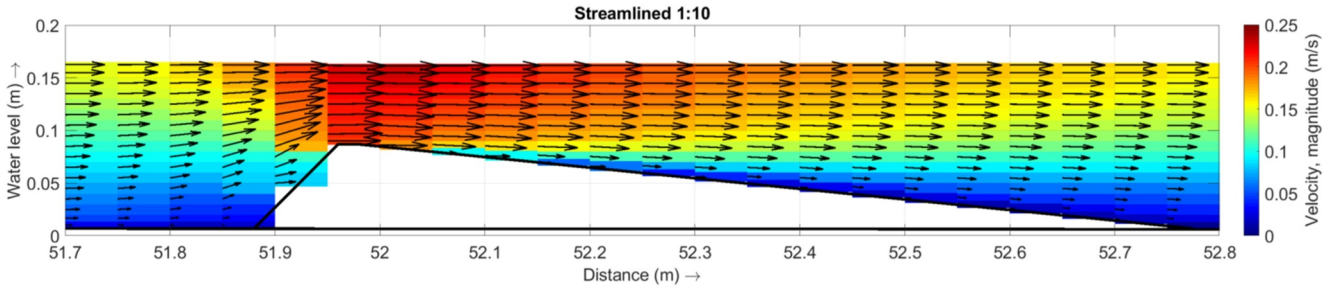

Figure 11. Flow velocity contours and vectors over a groyne at $y = 2.25$ m after streamlining the downstream face to 1V:10H (case h160).

meshes. The computed effects on water levels were compared with the results from flume experiments of the Bundesanstalt für Wasserbau. Although the standard approach (2DH-C model) showed reasonable performance, it leaves room for improvement. After calibration, it gave good predictions of water levels at flow conditions close to the calibrated conditions. We also compared simulations of the flow over a groyne and the flow over a weir (3D-NH vs. 2DV-F). Despite the obvious differences in the flow fields, the flows over weirs and over groynes resulted in similar resistance values and flow depths at every submergence level. This shows that groynes can be modeled as subgrid weir elements in 2DH models for design flood conditions as long as flow over submerged weirs can be simulated with a reliable method.

Among the alternative models, the 2DH-F model which defines groynes in the topography performed worse than the 2DH-C model in predicting the flow resistance. In the 2DH-C model, the 2D simulation was coupled with a 1D equation for groyne resistance. However, in the 2DH-F model, the groyne resistance was obtained from the physics by solving 2D momentum equations. Trying to model a highly 3D flow field by using a 2D modeling technique without subgrid correction fell short here. The 3D non-hydrostatic model, which is computationally the most expensive model, performed the best in predicting the water levels and the discharge distributions between the main channel and the groyne field. Its results deviated slightly from the observed water depths at the highest submergences. However, these slight deviations increased systematically with the increase in submergence of the groynes. The simulated downstream eddy was smaller than observed due to moderately accurate reproduction of vertical flow separation, which was linked with turbulence model capabilities or mesh size. The slight deviations in surface velocity predictions can be related to the mesh resolution. Although the mesh was fine from a river modeling perspective, it was coarse compared to meshes in CFD (Computational Fluid Dynamics) applications in hydraulics. The 3D hydrostatic model performed close to the 3D non-hydrostatic model, slightly diverging from the measured values. This makes it the second-best model after 3D-NH while being computationally less expensive. The computational power required by the 3D models was 26–650 times larger than the ones required by the 2D models. The computational facilities of the user and the available time thus determine the selection of the modeling approach.

Groyne modifications were simulated by using 3D-NH and 2DH-C. For both lowering and streamlining the groynes, the hydraulic resistance decreased non-linearly with the amount of lowering and streamlining. Lowering was most effective in the first two cm, while streamlining by flattening the downstream groyne slope from 1V:1.5H to 1V:5H seemed more effective than flattening from 1V:5H to 1V:10H. The lack of experimental data

Figure 12. Natural streamlining of groynes along the Nederrijn River at Arnhem (km 880.4) by lee-side deposition of sand during floods. Photographs taken on 6 March 2021 after flood with 7,395 $m^3 s^{-1}$ peak discharge at Lobith gauge station (approximate return period: 5 years) on 8 February 2021 (courtesy Tom Buijse).

did not allow further validation of model performances in simulating the effects of groyne modifications. The 3D-NH model was found more reliable and the performance of the standard model (2DH-C) was assessed by referencing to the 3D-NH model results.

Data Availability Statement

The experimental data for this research is not publicly available due to institutional reasons. Data is stored in this in-text data citation reference: Baron M. (2013): Kalibrierung und Validierung der numerischen Verfahren Telemac und UnTRIM anhand einer Laborrinne, Internal Report of Bundesanstalt für Wasserbau (BAW) (In German). Delft3D is an open-source software which is available online through the developer's website (Deltares (2024). Delft3D flow: User manual. Deltares. https://oss.deltares.nl/web/delft3d/downloads). We used Delft3D (flow2d3d, version 6.02.13.7545) to construct and execute the numerical model. Model related figures were also developed by using Delft3D. Model properties are defined in this paper. The inlet and outlet boundary conditions were used the same as the physical experiments (Table 1 of the present paper).

Notation

g gravitational acceleration

H_1 upstream flow depth of a submerged weir;

H_2 downstream flow depth of a submerged weir;

h flow depth;

k turbulent kinetic energy;

P Vilemonte formula fit parameter;

Q water discharge;

S submergence rate;

x horizontal space coordinate in the main flow direction

y horizontal space coordinate in the direction lateral to the main flow

ε rate of viscous dissipation;

ν kinematic viscosity of fluid;

ρ density of fluid.

Acknowledgments
We would like to thank Bundesanstalt für Wasserbau (BAW) for providing us their experimental data. We gratefully acknowledge Robert Jan Labeur and Wim Uijttewaal for their advice, and Frank Platzek for his advice and making experimental data from BAW available for this study. The first author of this study (B. Y.) acknowledges the support of a post-doctoral grant from The Scientific and Technical Research Council of Turkey (TUBITAK, Grant 2219).

References

Ali, S. (2013). *Flow over weir-like obstacles*. Dissertation. Delft University of Technology.

Ambagts, L. R. (2019). *Flow over and around submerged groynes—numerical modelling and analysis of a groyne flume experiment*. MSc Thesis. Delft University of Technology.

Baron, M. (2013). *Kalibrierung und Validierung der numerischen Verfahren Telemac und UnTRIM anhand einer Laborrinne [Calibration and validation of the numerical methods Telemac and UnTRIM using a laboratory flume]*. [In German]. Internal Report of Bundesanstalt für Wasserbau (BAW).

Bloemberg, G. (2001). *Stroomlijnen van zomerkaden [streamlining of summer dikes]*. [In Dutch]. MSc Thesis. Delft University of Technology.

Bos, M. G. (1989). *Discharge measurement structures, Publication 20*. International Institute for Land Reclamation and Improvement.

Chanson, H. (2004). *The hydraulics of open channel flow* (2 ed.). Wiley.

Deltares. (2014). *Delft3D flow: User manual*. Deltares.

Deltares. (2024). Delft3D [Computer software]. Retrieved from https://oss.deltares.nl/web/delft3d/downloads

Duc, B. M., Wenka, T., & Rodi, W. (2004). Numerical modeling of bed deformation in laboratory channels. *Journal of Hydraulic Engineering*, *130*(9), 894–904. https://doi.org/10.1061/(asce)0733-9429(2004)130:9(894)

Forester, C. K. (1977). Higher order monotonic convective difference schemes. *Journal of Computational Physics*, *23*(1), 1–22. https://doi.org/10.1016/0021-9991(77)90084-5

Fritz, H. M., & Hager, W. H. (1998). Hydraulics of embankment weirs. *Journal of Hydraulic Engineering*, *124*(9), 963–971. https://doi.org/10.1061/(ASCE)0733-9429(1998)124:9(963)

Gerritsen, H., de Goede, E. D., Platzek, F. W., Genseberger, M., van Kester, J. A. T. M., & Uittenbogaard, R. E. (2008). Validation document Delft3D-FLOW; A software system for 3D flow simulations. The Netherlands: Delft HydraulicsReport X0356, M3470.

Glas, M., Glock, K., Tritthart, M., Liedermann, M., & Habersack, H. (2018). Hydrodynamic and morphodynamic sensitivity of a river's main channel to groyne geometry. *Journal of Hydraulic Research*, *56*(5), 714–726. https://doi.org/10.1080/00221686.2017.1405369

Glock, K., Tritthart, M., Gmeiner, P., Pessenlehner, S., & Habersack, H. (2017). Evaluation of engineering measures on the Danube based on numerical analysis. *Journal of Applied Water Engineering and Research*, *7*(1), 48–66. https://doi.org/10.1080/23249676.2017.1355757

Hager, W., & Schwalt, M. (1994). Broad-crested weir. *Journal of Irrigation and Drainage Engineering*, *120*(1), 13–26. https://doi.org/10.1061/(ASCE)0733-9437(1994)120:1(13)

Havinga, H. (2020). Towards sustainable river management of the Dutch Rhine River. *Water*, *12*(6), 1827. https://doi.org/10.3390/w12061827

Hüsener, T. (2015). *Hydraulisch-morphologische laboruntersuchungen an stromregelungsbauwerken [Hydraulic-morphological laboratory tests on flow control structures]*. [In German]. 38. Dresdner Wasserbaukolloquium Dresden (pp. 79–88). Technische Universität Dresden, Institut für Wasserbau und Technische Hydromechanik. Retrieved from https://hdl.handle.net/20.500.11970/103368

Hüsener, T., Faulhaber, P., & Baron, M. (2012). *Modifikationen in bestehenden Stromregelungssystemen an Wasserstraßen - Untersuchung mit gegenständlichen und numerischen Verfahren [Modifications in existing flow control systems on waterways - investigation with objective and numerical methods]*. [In German] In: Wasser, Energie, global denken lokal handeln: Wasserbausymposium (pp. 395–402). Graz, Technische Universität Graz. Retrieved from https://hdl.handle.net/20.500.11970/100819

Huthoff, F., Pinter, N., & Remo, J. W. (2013). Theoretical analysis of wing dike impact on river flood stages. *Journal of Hydraulic Engineering*, *139*(5), 550–556. https://doi.org/10.1061/(ASCE)HY.1943-7900.0000698

Jeon, J., Lee, J. Y., & Kang, S. (2018). Experimental investigation of three-dimensional flow structure and turbulent flow mechanisms around a nonsubmerged spur dike with a low length-to-depth ratio. *Water Resources Research*, *54*(5), 3530–3556. https://doi.org/10.1029/2017wr021582

Jongeling, T., van Kester, J., & Goede, E. (2010). *Stroomlijnen van kribben in WAQUA [streamlining of groynes in WAQUA]*. Deltares. [In Dutch] memo 1002047-000-ZWS-0012.

Kang, S., Hill, C., & Sotiropoulos, F. (2016). On the turbulent flow structure around an instream structure with realistic geometry. *Water Resources Research*, *52*(10), 7869–7891. https://doi.org/10.1002/2016wr018688

Kashyap, S., Rennie, C. D., Townsend, D. R., Constantinescu, G., & Tokyay, T. (2010). Flow around submerged groynes in a sharp bend using a 3D LES model. *River Flow*, 643–650. https://hdl.handle.net/20.500.11970/99700

Klijn, F., Asselman, N., & Mosselman, E. (2018). Robust river systems: On assessing the sensitivity of embanked rivers to discharge uncertainties, exemplified for The Netherlands' main rivers. *Journal of Flood Risk Management*, *12*(S2), e12511. https://doi.org/10.1111/jfr3.12511

Koken, M., & Constantinescu, G. (2011). Flow and turbulence structure around a spur dike in a channel with a large scour hole. *Water Resources Research*, *47*(12), W12511. https://doi.org/10.1029/2011wr010710

Launder, B. E., & Spalding, D. B. (1974). The numerical computation of turbulent flows. *Computer Methods in Applied Mechanics and Engineering*, *3*(2), 269–289. https://doi.org/10.1016/0045-7825(74)90029-2

Mosselman, E. (2004). "Numerical modeling of bed evolution in channel bends" (discussion). *Journal of Hydraulic Engineering*, *130*(1), 82. https://doi.org/10.1061/(asce)0733-9429(2004)130:1(82)

Mosselman, E. (2018). Modelling in applied hydraulics: More accurate in decision-making than in science? Chapter 53. In Ph. Gourbesville, J. Cunge, & G. Caignaert (Eds.), *Advances in Hydroinformatics; SimHydro 2017—Choosing the right model in applied hydraulics* (pp. 741–749). Springer. https://doi.org/10.1007/978-981-10-7218-5_53

Mosselman, E. (2022). The Dutch Rhine branches in the Anthropocene – Importance of events and seizing of opportunities. *Geomorphology*, *410*, 108289. https://doi.org/10.1016/j.geomorph.2022.108289

Mosselman, E., & Struiksma, N. (1992). *Effecten van kribverlaging [Effects of lowering the groynes]*. [In Dutch] Internal Technical Report. WL| Delft Hydraulics.

Rijkswaterstaat. (n.d.). Room for the River Project. Retrieved from https://www.rijkswaterstaat.nl/english/water/water-safety/room-for-the-rivers/index.aspx

Rodi, W. (2017). *Turbulence models and their application in hydraulics: A state-of-the-art review*. Routledge.

Stelling, G. S., & Leendertse, J. J. (1992). Approximation of convective processes by cyclic AOI methods. In *Estuarine and coastal modeling* (pp. 771–782). ASCE.

Tritthart, M., Liedermann, M., & Habersack, H. (2009). Modelling spatio-temporal flow characteristics in groyne fields. *River Research and Applications*, *25*(1), 62–81. https://doi.org/10.1002/rra.1169

van Broekhoven, R. W. A. (2007). *Het effect van kribverlaging op de afvoercapaciteit van de Waal ten tijde van hoogwater [The effect of groyne lowering on the discharge capacity of the Waal during high water]*. [In Dutch]. Graduation Report. Delft University of Technology.

van Stokkom, H. T. C., Smits, A. J. M., & Leuven, R. S. E. W. (2005). Flood Defense in The Netherlands. *Water International*, *30*(1), 76–87. https://doi.org/10.1080/02508060508691839

Villemonte, J. R. (1947). Submerged-weir discharge studies. *Engineering News-Record*, 866–869.

Williams, T. G., Guikema, S. D., Brown, D. G., & Agrawal, A. (2020). Assessing model equifinality for robust policy analysis in complex socio-environmental systems. *Environmental Modelling and Software*, *104831*, 104831. https://doi.org/10.1016/j.envsoft.2020.104831

Xiang, K., Yang, Z., Wu, S., Gao, W., Li, D., & Li, Q. (2020). Flow hydrodynamics of the mixing layer in consecutive vegetated groyne fields. *Physics of Fluids*, *32*(6), 065110. https://doi.org/10.1063/5.0006317

Yossef, M. F. M. (2005). *Morphodynamics of rivers with groynes*. PhD Thesis. Delft University of Technology.

Yossef, M. F. M. (2017). *Hydraulic modelling of standard and streamlined groynes. Internal Technical Report*. Deltares.

Yossef, M. F. M., & de Vriend, H. J. (2011). Flow details near river groynes: Experimental investigation. *Journal of Hydraulic Engineering*, *137*(5), 504–516. https://doi.org/10.1061/(ASCE)HY.1943-7900.0000326

Zagonjolli, M., Platzek, F., & van Kester, J. (2017). *Modelling the flow over a groyne and weir in WAQUA*. Internal Technical Report. Deltares.